Optical antenna enhanced spontaneous emission

Michael S. Eggleston[a], Kevin Messer[a], Liming Zhang[b], Eli Yablonovitch[a,1], and Ming C. Wu[a,1]

[a]Electrical Engineering and Computer Sciences Department, University of California, Berkeley, CA 94720; and [b]Bell Labs, Alcatel-Lucent, Holmdel, NJ 07733

Contributed by Eli Yablonovitch, December 12, 2014 (sent for review November 17, 2014)

Atoms and molecules are too small to act as efficient antennas for their own emission wavelengths. By providing an external optical antenna, the balance can be shifted; spontaneous emission could become faster than stimulated emission, which is handicapped by practically achievable pump intensities. In our experiments, InGaAsP nanorods emitting at ∼200 THz optical frequency show a spontaneous emission intensity enhancement of 35× corresponding to a spontaneous emission rate speedup ∼115×, for antenna gap spacing, d = 40 nm. Classical antenna theory predicts ∼2,500× spontaneous emission speedup at d ∼ 10 nm, proportional to $1/d^2$. Unfortunately, at d < 10 nm, antenna efficiency drops below 50%, owing to optical spreading resistance, exacerbated by the anomalous skin effect (electron surface collisions). Quantum dipole oscillations in the emitter excited state produce an optical ac equivalent circuit current, $I_o = q\omega|x_o|/d$, feeding the antenna-enhanced spontaneous emission, where $q|x_o|$ is the dipole matrix element. Despite the quantum-mechanical origin of the drive current, antenna theory makes no reference to the Purcell effect nor to local density of states models. Moreover, plasmonic effects are minor at 200 THz, producing only a small shift of antenna resonance frequency.

nanophotonics | metal optics | plasmonics | ultrafast devices

Antennas emerged at the dawn of radio, concentrating electromagnetic energy within a small volume $<<\lambda^3$, enabling nonlinear radio detection. Such coherent detection is essential for radio receivers and has been used since the time of Hertz (1). Conversely, an antenna can efficiently extract radiation from a subwavelength source, such as a small cellphone. Despite the importance of radio antennas, 100 y went by before optical antennas began to be used to help extract optical frequency radiation from very small sources such as dye molecules (2–10) and quantum dots (11–14).

In optics, spontaneous emission is caused by dipole oscillations in the excited state of atoms, molecules, or quantum dots. The main problem is that a molecule is far too small to act as an efficient antenna for its own electromagnetic radiation. Antenna length, l, makes a huge difference in radiation rate. An ideal antenna would preferably be $\lambda/2$, a half-wavelength in size. To the degree that an atomic dipole of length l is smaller than $\lambda/2$, the antenna radiation rate $\Delta\omega$ is proportional to $\omega(l/\lambda)^3$, as given by the Wheeler limit (15). Spontaneous emission from molecular-sized radiators is thus slowed by many orders of magnitude, because radiation wavelengths are much larger than the atoms themselves. Therefore, the key to speeding up spontaneous emission is to couple the radiating molecule to a proper antenna of sufficient size.

Since the emergence of lasers in 1960, stimulated emission has been faster than spontaneous emission. Now the opposite is possible. In the right circumstances, antenna-enhanced spontaneous emission could become faster than stimulated emission. Theoretically, very large bandwidth >100 GHz or >1 THz is possible when the light emitter is coupled to a proper optical antenna (16).

Metal optics have been able to shrink lasers to the nanoscale (17–20), but high losses in metal-based cavities make it increasingly difficult to achieve desirable performance. Metal structures have also been used to enhance the spontaneous emission rate, such as by coupling excited material to flat surface plasmon waves (21–28). Flat metal surfaces are far from ideal antennas, resulting in low radiation efficiencies and large ohmic losses. Semiconductor emitters have been further limited by large surface recombination losses and by processing difficulties at the extremely small dimensions. Semiconductor experiments (29, 30) show weak antenna–emitter coupling, with the antenna enhancement sometimes masked by metal-induced elastic scattering that enhances light extraction from the semiconductor substrate. Light extraction alone can increase optical emission by $4n^2$, as often used in commercial light-emitting diodes (LEDs), without necessarily modifying the spontaneous emission rate (31, 32).

In this article, we elucidate the physics of antenna-enhanced spontaneous emission, using a traditional antenna circuit model, not the Purcell effect (33) nor a local density-of-states model (34). We use the circuit approach to analyze for the maximum possible spontaneous emission enhancement in the presence of spreading resistance losses (35) and the nonlocal anomalous skin effect (36) in the metal.

We experimentally tested an optical dipole antenna, coupled to a "free-standing" 40-nm nanorod of semiconductor material. Thus far, optical emission measurements show a >115× antenna spontaneous emission rate enhancement factor compared with no antenna at all. At smaller dimensions, circuit theory predicts a spontaneous emission rate enhancement $>10^4\times$, but at the penalty of decreased antenna efficiency. Nonetheless, we will derive that >2,500× rate enhancement should be possible, while still maintaining antenna efficiency >50%.

Antenna Physics

An antenna converts free space electromagnetic waves to ac currents in circuits and vice versa. At radio frequencies and at optical frequencies the antenna physics are quite similar. There are three important questions about antennas:

Significance

Since the invention of the laser over 50 y ago, stimulated emission has been stronger and far more important than spontaneous emission, the ordinary light we are accustomed to. Indeed spontaneous emission has been looked down upon as a weak effect. Now a new science of enhanced spontaneous emission is emerging that makes spontaneous emission faster than stimulated emission. This new science depends upon the use of optical antennas to increase the spontaneous emission rate. Antennas emerged at the dawn of radio for concentrating electromagnetic energy to a small volume. Despite the importance of radio antennas, 100 y went by before optical antennas began to be used to help extract optical frequency radiation from very small sources such as dye molecules and quantum dots.

Author contributions: M.S.E., E.Y., and M.C.W. designed research; M.S.E. and K.M. performed research; M.S.E., K.M., E.Y., and M.C.W. analyzed data; L.Z. contributed new reagents/analytic tools; M.S.E. and E.Y. wrote the paper; and L.Z. provided metalorganic chemical vapor deposition epitaxial material.

The authors declare no conflict of interest.

Freely available online through the PNAS open access option.

[1]To whom correspondence may be addressed. Email: eliy@eecs.berkeley.edu or wu@eecs.berkeley.edu.

This article contains supporting information online at www.pnas.org/lookup/suppl/doi:10.1073/pnas.1423294112/-/DCSupplemental.

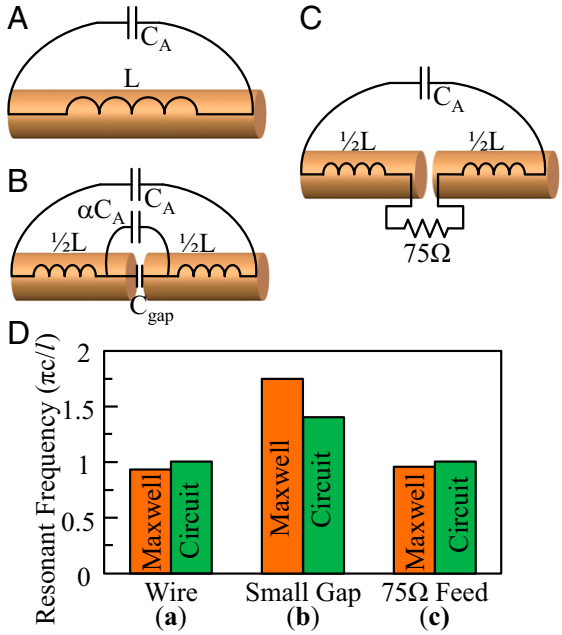

Fig. 1. Circuit models for common antenna geometries. (*A*) A straight wire. (*B*) A straight wire with a center gap, where a molecule or quantum dot could be inserted. (*C*) The case of a straight wire with a 75Ω load at the center. (*D*) The fundamental resonance frequency is in units of $\pi c/l$, where l is the wire length. Orange bars are calculated from Maxwell's equations and green bars from a circuit model. In the calculation, the wire length l =1.5 m, the wire diameter = $2r$ = 1 mm, and the gap spacing = 0.5 mm. The metal conductivity was taken to be 4.56×10^5/Ωcm, which at 100 MHz translates to a complex dielectric constant, $\varepsilon_m = 1 - j8.2 \times 10^9$. From Table 1, $L = (\mu_o/\pi^2)l \times \ln(l/r) = 1.4\ \mu H$, $C_A = \varepsilon_A l \times \ln(l/r) = 1.82$ pF, $C_{gap} = \varepsilon_g \pi r^2/d = 55.6$ fF. The stray capacitance of the wire region adjacent to the gap is αC_A, where $\alpha = 1$.

i) For a given rms ac current, $I_{rms}(\omega)$, how much electromagnetic wave power P will be launched? Because radiated power is proportional to current squared, the question reduces to finding the coefficient R in $P = I^2R$, where $R \equiv R_{radiation}$ or R_{rad} is called radiation resistance. $R_{radiation} = (2\pi/3)(l/\lambda)^2\sqrt{(\mu_o/\varepsilon_o)}$ for constant current in a wire length l, where $\sqrt{(\mu_o/\varepsilon_o)} \sim 377\Omega$ is the fundamental impedance of free space. $R_{radiation}$ is derived in most antenna books (37, 38).

ii) What is the cross-section for an antenna capturing electromagnetic wave power from free space optical intensity and transferring it to a matched load? Surprisingly, antenna capture cross-section has a universal answer for all antennas, no matter how small: $Area = \lambda^2/\Omega$, where λ is the resonant electromagnetic wavelength, and Ω is the acceptance solid angle of the antenna. $\Omega = 4\pi$ steradians for an isotropic antenna leading to a capture cross-section $Area = \lambda^2/4\pi$, whereas for dipoles $\Omega = (2/3)4\pi = 8\pi/3$ steradians, because z-directed radiation parallel to the dipole is forbidden, whereas x and y are allowed. A more highly directive antenna captures proportionately more power from an incident plane wave. By time reversal, captured power $P \equiv Intensity \times Area$ equals reradiated power $= I^2R_{radiation} = V^2/R_{radiation}$. Thus, in a receiving antenna, there is an effective optical frequency voltage source $V_{rms}(\omega) = 2\sqrt{(Intensity \times Area \times R_{radiation})}$, where the 2 accounts for voltage division between $R_{radiation}$ and matched R_{load}. With $R_{load} = 0$, the reradiation cross-section $Area = 3\lambda^2/2\pi$. The equivalent circuit of a transmitting antenna will be shown (see Fig. 3).

iii) Every metallic structure is resonant at some frequency and is, in effect, an LC resonator, with distributed inductance L and capacitance C. Because self-oscillating currents lead to some electromagnetic radiation, every metal object is also an antenna. In optics we often seek the highest possible Q factor, but in antennas we seek the opposite because we desire radiation losses. Harold Wheeler (15) answered the question, What is the lowest Q factor that can be achieved in an antenna? This is called the Wheeler limit: $(\omega/\Delta\omega) \equiv Q \sim (3/4\pi^2)(\lambda/l)^3$, where l is the longest linear dimension of the antenna.

Thus, a small antenna is a poor antenna, with a high Q, but nonetheless still capturing over an $Area \sim \lambda^2/4\pi$, which can actually be much larger than its physical area. For example, a dipole atom is a very small resonator and has a high Q according to the Wheeler limit, but it scatters electromagnetic waves with a cross-sectional area, $Area = 3\lambda^2/2\pi$, much larger than the atomic size.

The lowest LC resonant frequency of a metallic object is usually related to its size. That is only the first of many electromagnetic resonances that extend all of the way to high optical frequencies, at which point the resonances could be influenced by kinetic inductance and assume some plasmonic character.

The oscillating ac currents associated with the LC resonators can radiate electromagnetic energy. Thus, all metal objects act as antennas to some degree, converting ac currents to radiated power.

For a given resonance, there is insight to be gained by visualizing the distributed inductance and capacitance as a circuit. In Fig. 1*A* we illustrate an LC_A circuit model associated with the lowest resonance of a straight wire, with $C_A = \varepsilon_A l \times \ln(l/r)$ modeling the tip-to-tip capacitance of the wire, as documented in

Table 1. Antenna circuit parameters

Gap capacitance		Current induced in antenna	
Blunt tips (39)	$C_{gap} = \frac{\varepsilon_g A}{d}$	Parallel plate current induced by ac dipole (40)	$I_0 = \frac{q\omega x_0}{d}$
Round tips (41)	$C_{gap} = \frac{\pi\varepsilon_g r}{2}\left[ln\left(\frac{r}{d}\right) + 2\gamma\right]$		
Lumped reactance terms		**Resistance terms**	
Faraday (38) inductance	$L_f = \frac{\mu_o}{\pi^2} l \times \ln\left(\frac{l}{r}\right)$	Radiation (38) resistance	$R_{rad} = \frac{2\pi}{3} Z_o \left(\frac{l_{eff}}{\lambda}\right)^2 n_A$
Kinetic (42) inductance	$L_k = \frac{l_{eff}}{A} Re\left\{\frac{1}{\omega^2\varepsilon_o(1-\varepsilon_m)}\right\}$	Ohmic (42) resistance	$R_{ohmic} = \frac{l_{eff}}{A} Im\left\{\frac{1}{\omega\varepsilon_o(1-\varepsilon_m)}\right\}$
Antenna (38) capacitance	$C_A = \frac{\varepsilon_A l}{\ln\left(\frac{l}{r}\right)}$	Spreading (35, 42) resistance	$R_{spread} = \frac{1}{\beta d} Im\left\{\frac{1}{\omega\varepsilon_o(1-\varepsilon_m)}\right\}$

Shown are circuit parameters of wire antennas, where r = wire radius, l = antenna length, l_{eff} = effective antenna length accounting for current → 0 at ends; for a half-wave antenna $l_{eff} = 0.64l$; A = antenna wire cross-sectional area, $Z_o \equiv \sqrt{(\mu_o/\varepsilon_o)}$, the impedance of free space; x_o = optical ac peak dipole moment length centered in a gap-spacing d; βd is the diameter on the adjacent electrodes over which the dipole currents spread (β = 1.6 for flat electrodes); n_A and ε_A are the refractive index and dielectric constant of the medium surrounding the antenna; ε_m = metal relative dielectric constant; and ε_g = dielectric constant in the gap.

Table 1. Fig. 1*B* illustrates the corresponding circuit model for a wire with a gap in the center, where a radiating atom or molecule can be inserted. Unfortunately, the narrow gap makes it notoriously difficult to accurately calculate the resonant frequency by analytical or numerical methods. The center capacitance includes the obvious parallel-plate capacitance $C_g = \varepsilon_g \pi r^2/d$ formed across the gap, but it also includes some of the stray capacitance αC_A of the wire region adjacent to the gap. Fig. 1*C* shows the circuit model for a wire driven by a 75Ω transmission line, which is equivalent to a 75Ω resistor in the center of the wire, increasing damping losses.

Each of these metallic structures in Fig. 1 *A–C* has its own fundamental resonance frequency given by the bar chart in Fig. 1*D*. The orange bar is calculated by solving Maxwell's equations, using Lumerical or CST software, and the green bar is solved from a circuit model with component values given in Fig. 1 and Table 1 with $\alpha C_A = C_A$ as the stray capacitance.

There are various loss mechanisms that must be added to the circuit models in Fig. 1. These can be represented as resistances as shown in Fig. 2. Radiation resistance is a desirable loss mechanism, whereas ohmic losses are undesirable. The radiation resistance is given in Table 1. The primary ohmic resistance of the antenna mode is given by the wire resistance, $R_{\text{ohmic}} = \rho(l_{\text{eff}}/A)$, where the optical resistivity is $\rho = \text{Im}\{1/\omega\varepsilon_o(1-\varepsilon_m)\}$.

For spontaneous emission, the antenna is driven by an emitter material that can be modeled as an oscillating dipole. Ramo's theorem (40) can then be used to calculate the amount of current induced on the antenna arms (an alternate method of calculating the antenna enhancement is given in ref. 43). For a parallel plate capacitor, the amount of current coupled into the antenna is $I_o = q\omega|x_o|/d$. It is therefore advantageous to shrink the gap d, to very small dimensions to increase the current coupled into the antenna. Unfortunately, at very small gap spacing, the fields of the driving dipole are confined to a very small region, βd, on the antenna tips. These fields give rise to current crowding before the current spreads out to the main antenna arm. This very high concentration of current at the feed gap of the antenna gives rise to an additional loss mechanism, spreading resistance. Although negligible at large gap spacing, spreading resistance becomes the dominant loss mechanisms for small gaps (Fig. 2*B*). A dipole that is a short distance $d/2$ from a metal surface will produce a corresponding current distribution spread over a diameter $\sim\beta d$, resulting in a total spreading resistance $R_{\text{spread}} = \rho/\beta d$ for both antenna arms in series. For dipoles centered between flat electrodes we find the dimensionless geometrical parameter $\beta = 1.6$.

The concentrated current also experiences a much shorter mean free path than electrons in the bulk of the antenna due to the anomalous skin effect (44), essentially surface collisions. This increases the effective metal resistivity in the concentrated current region, by the factor $(l_e + \delta d)/\delta d$, further exacerbating the spreading resistance, where l_e is the electron mean free path in the bulk metal, and δd is the surface collision mean free path, which scales with the concentrated current region size. Because δ requires a complicated nonlocal electrodynamic calculation, Fig. 2*B* simply plots the range $0.5 < \delta < 1$.

Fig. 2*B* shows how these loss mechanisms change with gap spacing. When the anomalous skin effect is included, spreading resistance eventually dominates all other loss mechanisms as the gap d is diminished. This unavoidable loss mechanism will ultimately limit the maximum efficiency of the antenna at high spontaneous emission enhancement.

These resistive losses appear in the circuit model shown in Fig. 3*A*, which is further simplified in Fig. 3*B*. The antenna spontaneous emission enhancement ratio measures the desired power in the radiation resistance arising from a driving dipole placed at the center of the feed gap, normalized to the power from a bare dipole. The antenna efficiency is power radiated divided by total power dissipated. These radiation characteristics can then be compared for antennas of different geometries. Fig. 4 shows the enhancement and efficiency of a rounded-tip dipole antenna having a gap filled with dielectric material typical of a semiconductor emitter (index $n = 3.4$). The solid curves in Fig. 4 are from the circuit model in Fig. 3*B*, and the dotted lines connecting squares represent a 3D finite difference time domain simulation (FDTD) of the same structure.

The large C_{gap} capacitance of a rectangular gap at narrow spacing effectively shorts out the current being driven into the antenna. The shorted current never sees the radiation resistance if $|1/\omega C_{\text{gap}}| < R_{\text{rad}}$.

We can remedy the drastic shunting of current across the gap, by reducing gap capacitance, for example by adopting hemispherical gap tips. If the tip radius of curvature is the same as the radius of the wire, the gap capacitance on close approach (41) is that of two spheres: $C_g = (\pi\varepsilon_g r/2)[\ln(r/d) + 2\gamma]$. This is only weakly logarithmically dependent on the r/d ratio. In Fig. 4, the rounded inner tips partially compensate for the higher-capacitance semiconductor filling.

The circuit model of Fig. 3 provides a closed-form solution for the antenna enhancement,

$$\text{Enhancement} = \frac{3}{2\pi}\left(\frac{\lambda_0}{d}\right)^2 \frac{R_{\text{rad}} Z_{\text{gap}}^2}{Z_0 (R_{\text{rad}} + R_{\text{ohmic}})^2},$$

where the enhancement is proportional to $1/d^2$, as has been previously shown (45). $Z_{\text{gap}} \equiv 1/j\omega(C_{\text{gap}} + \alpha C_A)$. From this it is clear

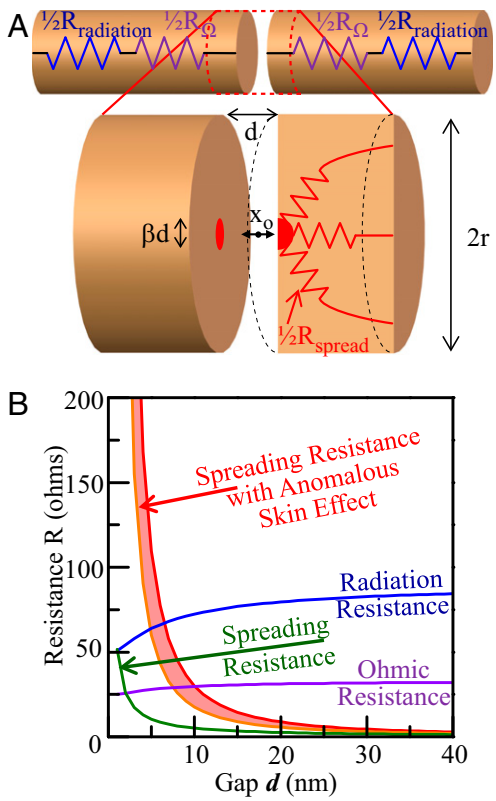

Fig. 2. Optical antenna resistance. (*A*) Schematic of a linear antenna (Au wire radius $r = 20$ nm) with a blunt vacuum gap showing the radiation resistance (blue), ohmic resistance (purple), and a zoom-in of the gap region highlighting the spreading resistance (red). (*B*) Plot of the radiation resistance (blue), ohmic resistance (purple), and spreading resistance (green) of a wire antenna as a function of gap spacing. For dipoles centered between flat electrodes the current is spread over a diameter $\beta d = 1.6d$. The effect of the anomalous skin effect is shown in the shaded red region bounded by $\delta = 1$ (orange) and by $\delta = 0.5$ (red). The antenna length l is adjusted to maintain 200 THz resonant frequency.

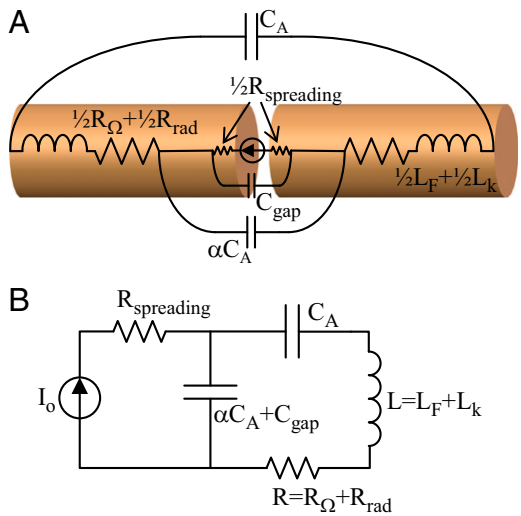

Fig. 3. Optical antenna circuit model. (*A*) Circuit components of an optical antenna, where R_Ω is the ohmic resistance, R_{rad} is the radiation resistance, L_k is the kinetic inductance, L_F is the Faraday inductance, C_{gap} is the internal gap capacitance $= \varepsilon_g \pi r^2/d$ for blunt tips of radius r, C_A is the external tip-to-tip capacitance, and αC_A is the stray capacitance between internal tips. We find $\alpha C_A \sim C_A$. (*B*) The same circuit in a simplified schematic.

that a small gap d is desired, but not to the point that $C_{gap} > \alpha C_A$. R_{rad} and $|1/\omega\alpha C_A|$ are closely related to Z_o. There is also an $R_{rad}/(R_{ohmic} + R_{rad})$ impedance matching term (46).

The efficiency from the circuit model of Fig. 3 is

$$\text{Efficiency} = \frac{R_{rad}}{R + R^2(C_A/L)(\alpha + C_{gap}/C_A)(1 + \alpha + C_{gap}/C_A)R_{spread}},$$

where $R \equiv R_{ohmic} + R_{rad}$. Neglecting the spreading resistance, R_{spread}, the efficiency is that of a normal resistive voltage divider. At small d, R_{spread} is increased by surface collisions (the anomalous skin effect), and R_{spread} limits the efficiency.

Experiment

To demonstrate antenna-enhanced spontaneous emission, many of our experiments have used the arch antenna, as shown in Fig. 5. This antenna works by introducing an inductor across the gap that can be used to diminish the effective gap capacitance of the antenna. InGaAsP is the spontaneous light-emitting material. The antenna was created by wet etching an InGaAsP film, parallel to crystal planes to create high aspect ratio sidewalls. The InGaAsP surface was coated with 3 nm TiO_2, using atomic layer deposition to provide electrical isolation between the InGaAsP surface and the gold antenna. Finally, a bar of gold was then deposited perpendicularly over the square nanorod to create the antenna and the inductor.

The fabricated structures were characterized by measuring the amount of light emitted. Increased spontaneous emission intensity, in competition with nonradiative losses, directly measures spontaneous emission enhancement. This measure of spontaneous emission rate is complementary to lifetime measurements. Lifetime can be influenced by emitters coupling to surface plasmons or optical cavities, which may not radiate, the energy still being lost as heat (21, 27), whereas the intensity method demands a knowledge of relative pump efficiency, relative emission pattern, and possible difference in internal quantum efficiency near the antenna.

In our experiment the dominant nonradiative mechanism is surface recombination. The quantum efficiency (QE) of the emitter is equal to the ratio of the radiative recombination rate to the surface recombination rate. With equivalent pumping and surface recombination conditions, an increase in optical emission is therefore a direct measurement of the increased rate of spontaneous emission into the far field. Although the nonradiative losses are undesirable in a device, they are a type of clock for fundamental measurements.

To ensure that nonradiative rates dominate, the InGaAsP surface was not treated with any form of passivation layer. Bare InGaAsP layers have been rigorously studied before and have been shown to have a surface recombination velocity of $\sim 3 \times 10^4$ cm/s (47, 48). Considering the ~34-nm width of the InGaAsP nanorods, this corresponds to a surface recombination lifetime of ~28 ps, which should be compared with InGaAsP's unenhanced spontaneous emission lifetime of >10 ns. The nanorods are covered in a 3-nm TiO_2 layer that increases the surface recombination rate by an additional factor of 3 (*Supporting Information*) and prevents direct contact between the InGaAsP and the gold antennas. This ensures that the only change in nonradiative recombination will be from ohmic losses in the antenna and not from changes in surface recombination. Although chemical surface passivation or cladding layers would greatly increase the light emission from this structure, they would impair the proper measurement of antenna properties, which is the main goal of this study.

It is also necessary to eliminate mechanisms that enhance external quantum efficiency without increasing the spontaneous emission rate, most notably improved light extraction. For a traditional LED, the majority of light gets trapped in the semiconductor and only a very small emission angle can escape. By using a textured surface or grating, the light extraction can be increased by up to $4n^2$, where n is the refractive index of the semiconductor (31). Arrays of optical antennas can provide scattering extraction enhancement, thereby increasing light output, but without increasing the emission rate. By completely removing the substrate and leaving only very small, subwavelength semiconductor islands, the possibility of scattering light extraction enhancement is removed.

To excite carriers in the semiconductor nanorods, a Ti:Sapphire laser at $\lambda = 720$ nm center wavelength, 120 fs pulse width, 13.3 MHz repetition rate, and 20 μW average power was focused onto the sample. The spot size of the pump laser was ~2 μm, within which approximately four devices were probed simultaneously. The pump was polarized off axis to the antenna to prevent antenna-enhanced pumping. Spontaneously emitted light was collected

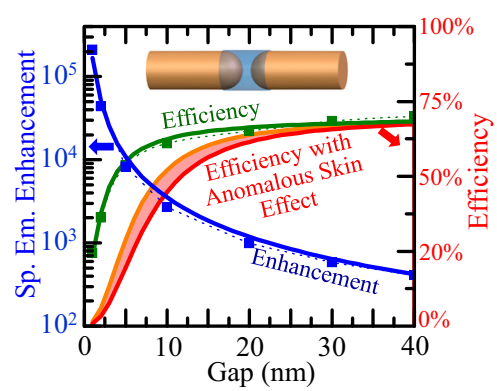

Fig. 4. Enhancement (blue) and efficiency (green) of an Au-wire antenna (radius r = 20 nm) with rounded inner tips and a semiconductor filled gap (light blue, refractive index = 3.4). The harmful effect of anomalous skin effect is plotted as the shaded red region bounded by $\delta = 1$ (orange) and by $\delta = 0.5$ (red). Solid lines are derived from the circuit model. Solid boxes connected by dotted lines are obtained from 3D FDTD simulations (CST; Lumerical). The antenna length l is adjusted to maintain 200 THz resonant frequency. For rounded electrodes, the current spreading factor $\beta \sim 0.5$ is a weak function of d/r in this range.

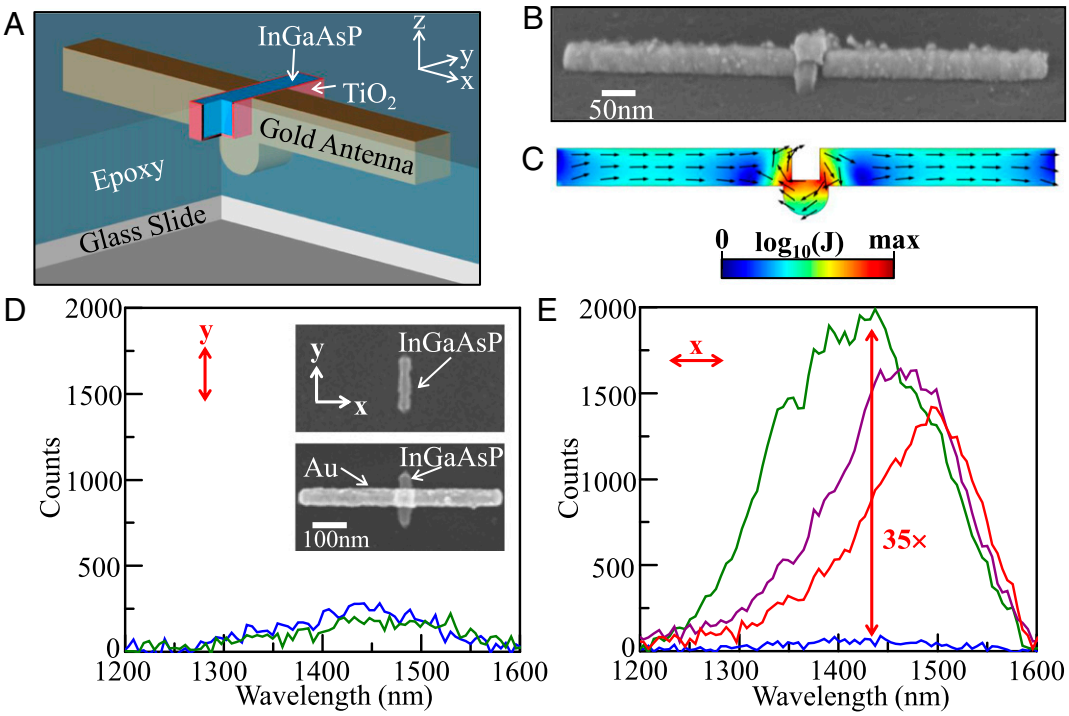

Fig. 5. Antenna-enhanced spontaneous emission from InGaAsP nanorods. (*A*) Schematic cutaway view of an arch-antenna–coupled InGaAsP nanorod, isolated by TiO_2, and embedded in epoxy. (*B*) Perspective SEM of antenna-coupled nanorod before substrate removal. (*C*) Current density of the arch-antenna electromagnetic mode showing the antiparallel current in the arch compared with the arms of the antenna. (*D*) Optical emission polarized in the unenhanced *y* direction for bare nanorod (blue) and antenna-coupled nanorod (green). (*Inset*) Top–down SEM image of antenna-coupled and bare nanorod. (*E*) Optical emission polarized in the enhanced *x* direction for a bare nanorod (blue) and from nanorods coupled to different antenna lengths: 400 nm (green), 600 nm (purple), and 800 nm (red) in length.

through the pump lens and passed through a polarizer to discriminate light polarized parallel or perpendicular to the antenna. The light was resolved by a spectrometer (Princeton Instruments Acton SP2300i) and detected on a cooled InGaAs CCD (Princeton Instruments OMA V).

Fig. 5*D* shows the optical emission spectrum collected for the two orthogonal emission polarizations for both the bare and the antenna-coupled InGaAsP nanorods. A 400-nm-long, 50-nm-wide antenna has little effect on the spontaneous emission polarized in the unenhanced direction, indicating that the presence of the antenna does not affect the pumping or surface recombination of the semiconductor nanorod. An improvement of 35×, however, is seen for light emitted polarized in the *x* direction (Fig. 5*E*) relative to the bare nanorod. The enhancement is spectrally broad, spanning almost 200 nm of vacuum wavelength, indicating an antenna Q on the order of ∼5. As the antenna arms are lengthened the antenna resonance red shifts and a corresponding shift in the enhanced spectrum can be observed. The red shift of the antenna resonance is affected by the LC matching arch. Longer antennas show spectral mismatch between the antenna resonance and the InGaAsP spontaneous emission peak.

Ideally, carriers generated in the nanorod would equilibrate with volume under the arch of the antenna, where the highest enhancement occurs. Unfortunately, the diffusion length is insufficient compared with the nanorod length. Because the recombination lifetime is limited to ∼10 ps by surface recombination, the diffusion length for holes in InGaAsP can be calculated as ∼16 nm, using 1/10th the bulk hole mobility of 10 cm^2/Vs (49). Consequently, a large portion of the carriers will never see the antenna arch before recombining. Given that the exposed InGaAsP arms are ∼50 nm long, compared with a diffusion length of ∼16 nm, only ∼32% of the carriers will diffuse to the antenna hotspot. Fabricating shorter nanorods will reduce this effect, but the devices in this study were limited by alignment tolerances. Taking this factor into consideration, the observed enhancement ratio of 35× corresponds to an actual enhancement greater than 115×.

Fig. 4 predicts an ∼400× enhancement factor for a 40-nm gap at the central vertex of the antenna. In the experiment, the optical electric field drops across ∼6 nm of TiO_2 before reaching the ∼34 nm of InGaAsP. Only a fraction of the antenna voltage drops across the semiconductor. The optical voltage division ratio is $34/(34 + 6\gamma) = 0.74$, where $\gamma \sim 2$ is the dielectric constant ratio of InGaAsP/TiO_2. Thus, the predicted 400× enhancement factor becomes $400(0.74)^2 \sim 220\times$, where light emission depends on electric field amplitude squared. The remaining experimental/theoretical discrepancy of ∼1/2 could be associated with spatial averaging away from the optimal central spot under the arch antenna.

Because half-wave antennas can have radiation $Q \sim 1$, radiation competes well with ohmic losses. We calculate an antenna efficiency of 66%.

In summary, we have demonstrated an enhanced spontaneous emission rate from InGaAsP nanorods coupled to an optical antenna, directly observing spontaneous emission intensity enhancement of 35×. This corresponds to a spontaneous emission rate enhancement of 115×.

Directly modulated semiconductor lasers are ∼200× faster than spontaneously emitting light-emitting diodes. If we can increase the optical antenna enhancement ratio to 200×, that will be a landmark in the competition between spontaneous emission and stimulated emission.

ACKNOWLEDGMENTS. This work was supported by the Center for Energy Efficient Electronics Sciences, National Science Foundation Award ECCS-0939514; by the Air Force Office of Scientific Research Project FA9550-09-1-0598; and by the Department of Energy Office of Basic Energy Sciences under Contract DE-AC02-05CH11231.

1. Mulligan JF (1989) Heinrich Hertz and the development of physics. *Phys Today* 42(3): 50–57.
2. Kinkhabwala A, et al. (2009) Large single-molecule fluorescence enhancements produced by a bowtie nanoantenna. *Nat Photonics* 3(11):654–657.
3. Muskens OL, Giannini V, Sánchez-Gil JA, Gómez Rivas J (2007) Strong enhancement of the radiative decay rate of emitters by single plasmonic nanoantennas. *Nano Lett* 7(9):2871–2875.
4. Bharadwaj P, Novotny L (2007) Spectral dependence of single molecule fluorescence enhancement. *Opt Express* 15(21):14266–14274.
5. Kuhn S, Mori G, Agio M, Sandoghdar V (2008) Modification of single molecule fluorescence close to a nanostructure: Radiation pattern, spontaneous emission and quenching. *Mol Phys* 106(7):893–908.
6. Bakker RM, et al. (2008) Nanoantenna array-induced fluorescence enhancement and reduced lifetimes. *New J Phys* 10(12):125022.
7. Busson MP, Rolly B, Stout B, Bonod N, Bidault S (2012) Accelerated single photon emission from dye molecule-driven nanoantennas assembled on DNA. *Nat Commun* 3:962.
8. Lee K-G, et al. (2012) Spontaneous emission enhancement of a single molecule by a double-sphere nanoantenna across an interface. *Opt Express* 20(21):23331–23338.
9. Zhang W, et al. (2012) Giant and uniform fluorescence enhancement over large areas using plasmonic nanodots in 3D resonant cavity nanoantenna by nanoimprinting. *Nanotechnology* 23(22):225301.
10. Novotny L, van Hulst N (2011) Antennas for light. *Nat Photonics* 5(2):83–90.
11. Farahani JN, Pohl DW, Eisler H-J, Hecht B (2005) Single quantum dot coupled to a scanning optical antenna: A tunable superemitter. *Phys Rev Lett* 95(1):017402.
12. Mertens H, Biteen JS, Atwater HA, Polman A (2006) Polarization-selective plasmon-enhanced silicon quantum-dot luminescence. *Nano Lett* 6(11):2622–2625.
13. Curto AG, et al. (2010) Unidirectional emission of a quantum dot coupled to a nanoantenna. *Science* 329(5994):930–933.
14. Chu X-L, et al. (2014) Experimental realization of an optical antenna designed for collecting 99% of photons from a quantum emitter. *Optica* 1(4):203–208.
15. Wheeler HA (1947) Fundamental limitations of small antennas. *Proc IRE* 35(12):1479–1484.
16. Lau EK, Lakhani A, Tucker RS, Wu MC (2009) Enhanced modulation bandwidth of nanocavity light emitting devices. *Opt Express* 17(10):7790–7799.
17. Hill MT, et al. (2007) Lasing in metallic-coated nanocavities. *Nat Photonics* 1(10):589–594.
18. Oulton RF, et al. (2009) Plasmon lasers at deep subwavelength scale. *Nature* 461(7264):629–632.
19. Yu K, Lakhani A, Wu MC (2010) Subwavelength metal-optic semiconductor nanopatch lasers. *Opt Express* 18(9):8790–8799.
20. Khajavikhan M, et al. (2012) Thresholdless nanoscale coaxial lasers. *Nature* 482(7384): 204–207.
21. Neogi A, et al. (2002) Enhancement of spontaneous recombination rate in a quantum well by resonant surface plasmon coupling. *Phys Rev B* 66(15):153305.
22. Okamoto K, et al. (2004) Surface-plasmon-enhanced light emitters based on InGaN quantum wells. *Nat Mater* 3(9):601–605.
23. Song J-H, Atay T, Shi S, Urabe H, Nurmikko AV (2005) Large enhancement of fluorescence efficiency from CdSe/ZnS quantum dots induced by resonant coupling to spatially controlled surface plasmons. *Nano Lett* 5(8):1557–1561.
24. Biteen JS, Lewis NS, Atwater HA, Mertens H, Polman A (2006) Spectral tuning of plasmon-enhanced silicon quantum dot luminescence. *Appl Phys Lett* 88(13):131109.
25. Fattal D, et al. (2008) Design of an efficient light-emitting diode with 10 GHz modulation bandwidth. *Appl Phys Lett* 93(24):243501.
26. Cho C-H, et al. (2011) Tailoring hot-exciton emission and lifetimes in semiconducting nanowires via whispering-gallery nanocavity plasmons. *Nat Mater* 10(9):669–675.
27. Sorger VJ, et al. (2011) Strongly enhanced molecular fluorescence inside a nanoscale waveguide gap. *Nano Lett* 11(11):4907–4911.
28. Russell KJ, Liu T-L, Cui S, Hu EL (2012) Large spontaneous emission enhancement in plasmonic nanocavities. *Nat Photonics* 6:459–462.
29. Arbel D, et al. (2011) Light emission rate enhancement from InP MQW by plasmon nano-antenna arrays. *Opt Express* 19(10):9807–9813.
30. Huang KCY, et al. (2012) Antenna electrodes for controlling electroluminescence. *Nat Commun* 3:1005.
31. Yablonovitch E (1982) Statistical ray optics. *JOSA* 72(7):899–907.
32. Joyce WB (1974) Geometrical properties of random particles and the extraction of photons from electroluminescent diodes. *J Appl Phys* 45(5):2229–2253.
33. Purcell EM (1946) Spontaneous emission probabilities at radio frequencies. *Phys Rev* 69(11-12):681.
34. Lai HM, Leung PT, Young K (1988) Electromagnetic decay into a narrow resonance in an optical cavity. *Phys Rev A* 37(5):1597–1606.
35. Gelmont B, Shur M (1993) Spreading resistance of a round ohmic contact. *Solid-State Electron* 36(2):143–146.
36. Kittel C, Fong CY (1987) *Quantum Theory of Solids* (Wiley, New York).
37. Kraus JD (1988) *Antennas* (McGraw-Hill, New York), 2nd Ed.
38. Sokolnikoff SA, Friis HT (1952) *Antennas: Theory and Practice* (Wiley, New York).
39. Jackson JD (1999) *Classical Electrodynamics* (Wiley, New York), 3rd Ed.
40. Ramo S (1939) Currents induced by electron motion. *Proc IRE* 27(9):584–585.
41. Lekner J (2011) Capacitance coefficients of two spheres. *J Electrostat* 69(1):11–14.
42. Staffaroni M, Conway J, Vedantam S, Tang J, Yablonovitch E (2012) Circuit analysis in metal-optics. *Photonics and Nanostructures - Fundamentals and Applications* 10(1): 166–176.
43. Mohammadi A, Sandoghdar V, Agio M (2008) Gold nanorods and nanospheroids for enhancing spontaneous emission. *New J Phys* 10(10):105015.
44. Gilberd PW (1982) The anomalous skin effect and the optical properties of metals. *J Phys F Met Phys* 12(8):1845–1860.
45. Eggleston M, Kumar N, Zhang L, Yablonovitch E, Wu MC (2012) Enhancement of photon emission rate in antenna-coupled nanoLEDs. *23rd IEEE International Semiconductor Laser Conference (ISLC)*, 10.1109/ISLC.2012.6348377.
46. Seok TJ, et al. (2011) Radiation engineering of optical antennas for maximum field enhancement. *Nano Lett* 11(7):2606–2610.
47. Sakai S, Umeno M, Amemiya Y (1980) Measurement of diffusion coefficient and surface recombination velocity for p-InGaAsP grown on InP. *Jpn J Appl Phys* 19(1):109–113.
48. Fukuda M (1986) Current drift associated with surface recombination current in InGaAsP/InP optical devices. *J Appl Phys* 59(12):4172–4176.
49. Pearsall TP (1982) *GaInAsP Alloy Semiconductors* (Wiley, New York).